View metadata, citation and similar papers at core.ac.uk

brought to you by CORE

provided by University of Strathclyde Institutional Repository

Zhang, Jiaying and McInnes, Colin R and Xu, Ming (2017) Reconfiguration of a smart surface using heteroclinic connections. Proceedings of the Royal Society A: Mathematical, Physical and Engineering Sciences. pp. 1-24. ISSN 1364-5021 , http://dx.doi.org/10.1098/rspa.2016.0614

This version is available at https://strathprints.strath.ac.uk/59036/

Strathprints is designed to allow users to access the research output of the University of Strathclyde. Unless otherwise explicitly stated on the manuscript, Copyright © and Moral Rights for the papers on this site are retained by the individual authors and/or other copyright owners. Please check the manuscript for details of any other licences that may have been applied. You may not engage in further distribution of the material for any profitmaking activities or any commercial gain. You may freely distribute both the url (https://strathprints.strath.ac.uk/) and the content of this paper for research or private study, educational, or not-for-profit purposes without prior permission or charge.

Any correspondence concerning this service should be sent to the Strathprints administrator: strathprints@strath.ac.uk

The Strathprints institutional repository (https://strathprints.strath.ac.uk) is a digital archive of University of Strathclyde research outputs. It has been developed to disseminate open access research outputs, expose data about those outputs, and enable the management and persistent access to Strathclyde's intellectual output.

Reconfiguration of a Smart Surface using Heteroclinic Connections

Jiaying Zhang[1, 2], Colin R McInnes[2] and Ming Xu[2, 3]

[1] Department of Mechanical and Aerospace Engineering, University of Strathclyde, Glasgow, G1 1XJ, United Kingdom

[2] School of Engineering, University of Glasgow, Glasgow, G12 8QQ, United Kingdom

[3] School of Astronautics, Beihang University, Beijing, 100083, People's Republic of China

E-mail: jiaying.zhang@strath.ac.uk

Abstract. A reconfigurable smart surface with multiple equilibria is presented, modelled using discrete point masses and linear springs with geometric nonlinearity. An energy-efficient reconfiguration scheme is then investigated to connect equal-energy unstable (but actively controlled) equilibria. In principle zero net energy input is required to transition the surface between these unstable states, compared to transitions between stable equilibria across a potential barrier. These transitions between equal-energy unstable states therefore form heteroclinic connections in the phase space of the problem. Moreover, the smart surface model developed can be considered as a unit module for a range of applications, including modules which can aggregate together to form larger distributed smart surface systems.

Keywords: Reconfigurable smart surface, heteroclinic connections, energy efficiency

1. Introduction

Many structures are designed with multi-stable characteristic for use in adaptive applications, such as compliant mechanisms. These structures have a number of advantages compared to conventional mechanisms, such as reducing the number of components required [1]. In particular, compliant mechanisms can use stored strain energy to enable motion from one stable position to another stable position [2]. The nonlinear deformation behaviour of such mechanisms has attracted significant interest with supporting experiment results [3]. Moreover, unstable equilibria could also be connected through heteroclinic connections in the phase space of the problem. Active control could be used to maintain the structure in unstable states, so that a transition between unstable configurations could be in principle found [4,5]. Transitions between equal-energy unstable states across a potential well are likely to be more efficient than transitions between stable states across a potential barrier. Meanwhile, the development of novel smart materials has helped to accelerate the implementation of practical adaptive structures, whose properties are controlled by external stimuli such as moisture, temperature, electric or magnetic fields [6,7]. A large number of smart materials with various characteristics, such as shape memory alloys (SMAs), temperature-responsive polymers (TMPs) and piezoelectric materials can in principle be used to fabricate such smart structures [8–10].

The increasingly broad application of smart structures can be found in many fields, such as the aerospace, energy and marine sectors, particularly for adaptive optics, vibration control and flow control [11]. Numerous engineering applications have also been investigated to utilise smart surfaces. For example, a reconfigurable reflector for a telecommunication satellite antenna has been investigated, providing significant advantages over conventional static antennae [12]. 'HoverMesh', a deformable structural mesh, has been developed as a spatial user interface. It has a cubical geometry with the upper wall designed as a deformable mesh of inflatable cells [13]. 'Smart skin' is a flexible, stretchable, and multifunctional surface which is fabricated from distributed sensing elements and electrodes. It has been applied in robotics and bionics and demonstrates excellent utility [14]. Moreover, some biomimetic concepts are derived from natural phenomenon, for example deployable membranes designed from folding tree leaves. New fold patterns were developed for applications to engineered structures by considering the folding of natural structures [15]. A shape memory alloy (SMA) assembly has also been developed as a mesh structure, which is attached to an inflatable boom. The smart mesh structure can then be used to control wrinkling and the deformed configuration of the inflatable boom structure [16]. A single sheet can be reconfigured to a range of desired shapes through multiple controllers and optimised design [17].

Furthermore, advanced applications have been considered by connecting smart surface units in order to enable additional states of the system. A compound surface has developed to investigate higher order

multi-stability through numerical simulation and experiment [18]. Others have designed materials that can alter their bulk shape through active control by the deformation of compliant elements. Such materials are best suited to high-precision applications that benefit from materials that can achieve a desired bulk surface profile rapidly and efficiently [19]. Moreover, deformable surfaces have been widely investigated in different concepts, such as morphing composites and multifunctional origami. Some optimised shape and stacking sequence fiber-reinforced polymer (FRP) shells have been developed to enhance their in-plane properties [20]. Meanwhile, the elastic instabilities of shells have also been studied to design geometries for modifying and controlling post-buckling behaviour of the structure [21]. A new passive honeycomb has been designed as a celluar structure, which is quite different to normal honeycomb structures. Based on an in-plane negative Poisson's ratio behaviour, a wing box filled with such a honeycomb has the ability to change the shape of an aerofoil [22]. The concept of using Poisson's ratio has been applied to the design of a Kirigami structure made of composite materials. Numerical and experimental results demonstrate such Kirigami cellular structures can easily implement shape changing behaviour based on their changeable deformation characteristics [23]. Other work is based on a negative Poisson's ratio, which uses a folded shell to produce Miura-ori fold patterns. Based on the kinematics of the folding, the structure can obtain the ability to perform planar deformations and bending. These folded shells have then been stacked together as Miura layers to produce a more complex 3D deployable structure which can have varying characteristics specific to different stacked configurations of the layers [24]. In addition, a double corrugation walled structure has been designed to offer an excellent ratio between bending and axial stiffness, which is the capabilty of concurrently carrying bending and shear loads for morphing skins [25]. Other smart surface work aims to develop a micro-scale system for conveying, sorting and positioning micro-parts. Such a smart surface is designed through distributed cells, which contain sensors, processing units and actuators [26].

In previous related work, McInnes and Waters investigated a simple smart structure model, which comprised a two mass chain with three springs [27]. The model was then approximated to provide a simple cubic nonlinearity to investigate its characteristics using dynamical system theory. A set of both stable and unstable equilibrium configurations were found, with transitions between the equal-energy unstable equilibria identified as heteroclinic connections. This cubic model was considered as a simple mechanical system with the ability to change its kinematic configuration between a finite set of unstable equilibria. The model was also used to investigate vibrational energy harvesting through the use of stochastic resonance [28].

In principle, such transitions between equal-energy unstable states can be achieved without energy input, in the absence of dissipation. Indeed simulation results show that reconfiguration between such unstable equilibria can be energetically more efficient compared to transitions between stable configurations, which need to cross a potential barrier. Moreover, a novel method has been investigated to plan and control such transitions based on a polynomial reference trajectory and an inverse control method. It is

envisaged that being computationally efficient, the control strategy could form the basis of real-time reconfiguration of smart structures [29]. Then, a more complex and realistic spring-mass model has been developed to better represent a more realistic smart structure system [30,31]. Again, a set of equilibria can be found which in principle can be connected with heteroclinic paths in the phase space of the problem. Strategies have also been considered to deal with energy dissipation using a range of control methods. The concept of heteroclinic connections between equal-energy unstable states has also been applied to reconfigure a linked bar mechanism [32].

In this paper heteroclinic connections are investigated as a means to reconfigure a simple discrete model of a smart surface structure, which is similar to the Hencky-type discrete model for pantographic structures. However, the work in this paper analyses the vertical deformation and so is quite different to the Hencky-type discrete model, which focuses on planar deformation [33]. In Section 2, the surface structure is considered as an elastic plane which has a range of both stable and unstable configurations. As an approximation, the surface is modelled as a two-dimensional spring-mass array without dissipation and with a simplifying cubic nonlinearity to allow an investigation of its characteristics using dynamical system theory. Firstly, Section 3 discusses each spring-mass element, considered as a cubic nonlinearity between different nodes, and then an adjacency matrix is used to assemble elements together. Therefore, a set of both stable and unstable equilibrium configurations can be identified in the model, so that the reconfiguration of the smart surface can be considered between the equal-energy unstable states, as presented in Section 4. It is assumed that the simple reconfigurable structure possesses embedded sensors and actuators to allow the unstable equilibria to be actively controlled. Meanwhile, a feedback control law is proposed that can stabilise the dynamics of the smart surface in Section 5. This control strategy can actively maintain the structure in an unstable configuration. Section 6 presents more complex dynamics of such surface structures, which can be formed from an assembly of modules. For example, each surface module can be regarded as a microsystem unit for conveying, sorting and positioning micro-parts.

2. Smart surface model

The smart surface structure consists of a two-dimensional array of connected springs and masses. Consider firstly a simple elastic model, with an array of masses connected as chains by linear springs of stiffness k and natural length L. In order to proceed, it is assumed that the masses can only move in the vertical (out-of-plane) direction without damping. The out-of-plane displacement of mass m is defined by displacement x, while each mass is separated by a fixed distance d. Consider a simple spring-mass element, which is the basic unit of the smart surface model. Based on the previous discussion, it is assumed that the masses can only move in the vertical direction as shown in Fig. 1.

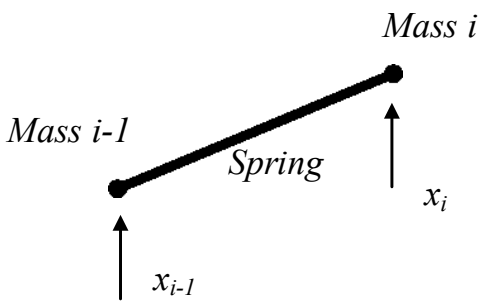

Figure 1. Spring-mass element.

To proceed, T is defined as the internal tension in a single spring, so that the tension of the spring can be described by

$$T = \Delta \cdot k \tag{1}$$

where Δ is the extension of the spring length beyond its natural length, which can be described by

$$\Delta = \sqrt{(x_{i-1} - x_i)^2 + d^2} - L \tag{2}$$

Therefore, the force experience by each node can be written as

$$f_{i,1} = -\Delta \cdot k \cdot \frac{(x_{i-1} - x_i)}{\sqrt{(x_{i-1} - x_i)^2 + d^2}} = -k(x_{i-1,} - x_i)\left(1 - \frac{l_0}{\sqrt{(x_{i-1} - x_i)^2 + d^2}}\right) \tag{3}$$

The dynamics of each mass in a 1-dimensional chain are then described by

$$m\ddot{x}_{i,1} = -k(x_{i-1} - x_i)\left(1 - \frac{l_0}{\sqrt{(x_{i-1} - x_i)^2 + d^2}}\right) \tag{4}$$

The nonlinear term can be expanded by assuming $x/d \ll 1$ to simplify the full nonlinearity of the problem. It can then be shown that

$$m\ddot{x}_i = -k\left(\frac{l_0}{d} - 1\right)(x_{i-1} - x_i) + \frac{kl_0}{2d^3}(x_{i-1} - x_i)^3 + \cdots \tag{5}$$

Following McInnes and Waters [27] a non-dimensional position coordinate $q = \sqrt{l_0/2d^3}\, x$ and non-dimensional time $\tau = t/\sqrt{m/k}$ can be defined with $\mu = (l_0/d - 1)$ so that

$$\ddot{q}_i = -\mu(q_{i-1} - q_i) + (q_{i-1} - q_i)^3 \tag{6}$$

In order to illustrate the smart surface model directly, a simple surface is considered as the structure shown in Fig. 2. The location of each mass as a row and column can be defined as u and v, respectively. Each mass $m_{i,j}$ can then be located on the ith row and j^{th} column, which is connected to its neighbours

by linear springs. The dynamics of mass $m_{i,j}$ are then driven by the displacements of $m_{i-1,j}, m_{i+1,j}, m_{i,j-1}$ and $m_{i,j+1}$. The dynamics of mass $m_{i,j}$ is therefore defined by

$$\begin{aligned}\ddot{q}_{i,j} = &-\mu(q_{i-1,j} - q_{i,j}) + (q_{i-1,j} - q_{i,j})^3 + \mu(q_{i,j} - q_{i+1,j}) - (q_{i,j} - q_{i+1,j})^3 \\ &- \mu(q_{i,j-1} - q_{i,j}) + (q_{i,j-1} - q_{i,j})^3 + \mu(q_{i,j} - q_{i,j+1}) - (q_{i,j} - q_{i,j+1})^3\end{aligned} \tag{7}$$

Due to the fixed boundary conditions of the problem, the surface model can be considered as a four degree-of-freedom system, which considers only vertical mass displacements. The displacement of the boundary nodes can be set to zero, i.e. $q_{0,0} = q_{0,1} = q_{0,2} = q_{0,3} = q_{1,0} = q_{1,3} = q_{2,0} = q_{2,3} = q_{3,0} = q_{3,1} = q_{3,2} = q_{3,3} = 0$. There dynamics of the full, coupled system can therefore be written as

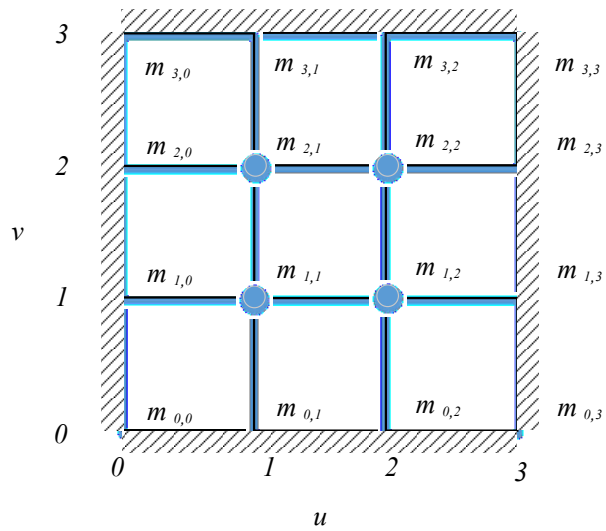

Figure 2. A simple surface model with fixed boundary condition.

$$\begin{bmatrix}\ddot{q}_{1,1}\\ \ddot{q}_{1,2}\\ \ddot{q}_{2,1}\\ \ddot{q}_{2,2}\end{bmatrix} = \begin{bmatrix}4\mu q_{1,1} - \mu(q_{2,1} + q_{1,2})\\ 4\mu q_{1,2} - \mu(q_{2,2} + q_{1,1})\\ 4\mu q_{2,1} - \mu(q_{1,1} + q_{2,2})\\ 4\mu q_{2,2} - \mu(q_{1,2} + q_{2,1})\end{bmatrix} + \begin{bmatrix}-2{q_{1,1}}^3 - (q_{1,1} - q_{2,1})^3 - (q_{1,1} - q_{1,2})^3\\ -2{q_{1,2}}^3 - (q_{1,2} - q_{2,2})^3 + (q_{1,1} - q_{1,2})^3\\ -2{q_{2,1}}^3 + (q_{1,1} - q_{2,1})^3 - (q_{2,1} - q_{2,2})^3\\ -2{q_{2,2}}^3 + (q_{1,2} - q_{2,2})^3 + (q_{2,1} - q_{2,2})^3\end{bmatrix} \tag{8}$$

This four degree-of-freedom system is easily formed from the dynamics of the problem through using Eq. (7). Moreover, the system is constructed from two parts, a linear destabilising force term and nonlinear stabilising force term. It can be expected that the linear and cubic terms will yield families of both stable and unstable equilibria.

3. General methods

We now consider a general method with an $n \times n$ array of masses using the same functional form of the nonlinearity above. It is again assumed that the system is considered conservative without dissipation. The adjacency matrix of the graph connecting the nodes can now be used to form the generalised position of each node. The four degree-of-freedom system above is firstly employed to

illustrate this general method. Since the system detailed above is considered conservative without dissipation, its behaviour can be described through the use of an effective potential $V(\boldsymbol{q},\mu)$ by the position set coordinate $\boldsymbol{q} = \{q_{i,j}\}$ $(i = 1 - n, j = 1 - n)$ such that the momenta $\boldsymbol{p} = \{p_{i,j}\}$ $(i = 1 - n, j = 1 - n)$ can be obtained from $\dot{p}_{i,j} = -\partial V(\boldsymbol{q},\mu)/\partial q_{i,j}$. The effective potential $V(\boldsymbol{q},\mu)$ can then be defined as

$$\begin{aligned} V(\boldsymbol{q},\mu) = {} & -\mu {q_{1,1}}^2 - \mu {q_{1,2}}^2 - \mu {q_{2,1}}^2 - \mu {q_{2,2}}^2 - \frac{1}{2}\mu\left(q_{1,1} - q_{2,1}\right)^2 - \frac{1}{2}\mu\left(q_{1,1} - q_{1,2}\right)^2 \\ & - \frac{1}{2}\mu\left(q_{1,2} - q_{2,2}\right)^2 - \frac{1}{2}\mu\left(q_{2,1} - q_{2,2}\right)^2 + \frac{1}{2}{q_{1,1}}^4 + \frac{1}{2}{q_{1,2}}^4 + \frac{1}{2}{q_{2,1}}^4 \\ & + \frac{1}{2}{q_{2,2}}^4 + \frac{1}{4}\left(q_{1,1} - q_{2,1}\right)^4 + \frac{1}{4}\left(q_{1,1} - q_{1,2}\right)^4 + \frac{1}{4}\left(q_{2,2} - q_{1,2}\right)^4 \\ & + \frac{1}{4}\left(q_{2,2} - q_{2,1}\right)^4 \end{aligned} \tag{9}$$

Equation (9) shows that the potential consists of two parts, one a quadratic term, which again provides a destabilising linear force at small displacements and a quartic term, which provides a stabilising, nonlinear restoring force at large displacements. It is assumed later that $q_{i,j}$ is a displacement that can be sensed and μ is a spring coupling parameter that can be manipulated for active control and stabilisation. Therefore, a general method can be considered such that the potential energy can be formed from two parts, a quadratic term and a quartic term, which can be defined by

$$M_2 = \begin{bmatrix} \left(q_{0,0} - q_{0,0}\right)^2 & \cdots & \left(q_{0,0} - q_{i,j}\right)^2 & \cdots & \left(q_{0,0} - q_{n,n}\right)^2 \\ \vdots & \ddots & \vdots & \ddots & \vdots \\ \left(q_{i,j} - q_{0,0}\right)^2 & \cdots & \left(q_{i,j} - q_{i,j}\right)^2 & \cdots & \left(q_{i,j} - q_{n,n}\right)^2 \\ \vdots & \ddots & \vdots & \ddots & \vdots \\ \left(q_{n,n} - q_{0,0}\right)^2 & \cdots & \left(q_{n,n} - q_{i,j}\right)^2 & \cdots & \left(q_{n,n} - q_{n,n}\right)^2 \end{bmatrix} \tag{10}$$

and

$$M_4 = \begin{bmatrix} \left(q_{0,0} - q_{0,0}\right)^4 & \cdots & \left(q_{0,0} - q_{i,j}\right)^4 & \cdots & \left(q_{0,0} - q_{n,n}\right)^4 \\ \vdots & \ddots & \vdots & \ddots & \vdots \\ \left(q_{i,j} - q_{0,0}\right)^4 & \cdots & \left(q_{i,j} - q_{i,j}\right)^4 & \cdots & \left(q_{i,j} - q_{n,n}\right)^4 \\ \vdots & \ddots & \vdots & \ddots & \vdots \\ \left(q_{n,n} - q_{0,0}\right)^4 & \cdots & \left(q_{n,n} - q_{i,j}\right)^4 & \cdots & \left(q_{n,n} - q_{n,n}\right)^4 \end{bmatrix} \tag{11}$$

where M is a $2n \times 2n$ matrix, the subscript '2' indicates the quadratic term and the subscript '4' indicates the quadratic term.

Then, an adjacency matrix is defined to form the generalised position of each node, which includes the relationship between every node by using an element '1' to define connected nodes and '0' to define unconnected nodes. Figure 3 illustrates a simple relationship between 4 nodes which are connected with one another sequentially in turn, thus the adjacency matrix can be defined by

$$A = \begin{bmatrix} 0 & 1 & 0 & 0 \\ 1 & 0 & 1 & 0 \\ 0 & 1 & 0 & 1 \\ 0 & 0 & 1 & 0 \end{bmatrix} \tag{12}$$

with the boundary conditions $q_1 = q_4 = 0$.

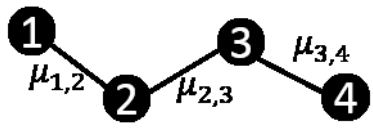

Figure 3. Example of a simple adjacency relationship.

In addition, a more general configuration can be considered by inserting the coupling parameters μ into the adjacency matrix, which express the detailed mechanical relationship between each of the nodes. The matrix A therefore can be rewritten as

$$A = \begin{bmatrix} 0 & \mu_{1,2} & 0 & 0 \\ \mu_{1,2} & 0 & \mu_{2,3} & 0 \\ 0 & \mu_{2,3} & 0 & \mu_{3,4} \\ 0 & 0 & \mu_{3,4} & 0 \end{bmatrix} \tag{13}$$

A generalised, extensive form of the adjacency matrix can now be defined as

$$A = \begin{bmatrix} 0 & \cdots & \mu_{00,i,j} & \cdots & \mu_{0,0,n,n} \\ \vdots & \ddots & \vdots & \ddots & \vdots \\ \mu_{00,i,j} & \cdots & 0 & \cdots & \mu_{i,j,n,n} \\ \vdots & \ddots & \vdots & \ddots & \vdots \\ \mu_{0,0,n,n} & \cdots & \mu_{i,j,n,n} & \cdots & 0 \end{bmatrix} \tag{14}$$

where $\mu_{i,j,n,n}$ defines the coupling relationship between nodes $q_{i,j}$ and $q_{n,n}$.

Accordingly, the potential energy of the system can be constructed by combining a quadratic-term matrix, quartic-term matrix and adjacency matrix. To proceed we define R as

$$R = R_1 \circ R_2 \tag{15}$$

where $\circ$ denotes the Hadamard product (element-wise product). The Hadamard product is an operation such that each element (ij) in the matrix is produced from the product of the corresponding location elements (ij) in another two matrices of the same dimension to generate a new matrix with the same dimension of the original two matrices. It is noted that R has the same dimension as the operands with R_1 and R_2.

Therefore, the total potential energy V can be defined as

$$V = -\frac{1}{2} sum(M_2 \circ A_1) + \frac{1}{4} sum\left(M_4 \circ A_\mu\right) \tag{16}$$

where A_1 and A_μ are upper triangular matrixes that can be developed from Eq.(12) and Eq.(14) such that

$$A_1 = \begin{bmatrix} \ddots & 1 & 1 \\ 0 & \ddots & 1 \\ 0 & 0 & \ddots \end{bmatrix} \tag{17}$$

$$A_\mu = \begin{bmatrix} 0 & \cdots & \mu_{00,i,j} & \cdots & \mu_{0,0,n,n} \\ \vdots & \ddots & \vdots & \ddots & \vdots \\ 0 & \cdots & 0 & \cdots & \mu_{i,j,n,n} \\ \vdots & \ddots & \vdots & \ddots & \vdots \\ 0 & \cdots & 0 & \cdots & 0 \end{bmatrix} \tag{18}$$

Since the system is considered conservative without dissipation, the Hamiltonian of the system can then be constructed from the kinetic and potential energy as

$$T(\boldsymbol{p}) = \frac{1}{2} \|\boldsymbol{p}^2\| \tag{19}$$

$$V(\boldsymbol{q}) = -\frac{1}{2} sum\left(M_2 \circ A_\mu\right) + \frac{1}{4} sum(M_4 \circ A_1) \tag{20}$$

where again the set $\boldsymbol{q} = \{q_{i,j}\}$ $(i = 1 - n, j = 1 - n)$ is associated with the set of momenta $\boldsymbol{p} = \{p_{i,j}\}$ $(i = 1 - n, j = 1 - n)$. Then the dynamics of the system can be obtained from Hamilton's equations. It is clear that since the kinetic energy is independent of $\boldsymbol{q}$, it can be seen that $\dot{\boldsymbol{p}} = -\nabla_q V(\boldsymbol{q})$ so that

$$\dot{q}_{i,j} = p_{i,j} \tag{21}$$

$$p_{i,j} = -\nabla_q V(\boldsymbol{q}) \tag{22}$$

The model shown in Fig.2 is now employed as an example to illustrate the detailed process using the general methods above. The labelled graph of the simple smart surface structure is shown in Fig. 4. The displacement of the boundary nodes can again be set to zero, i.e. $q_{0,0} = q_{0,1} = q_{0,2} = q_{0,3} = q_{1,0} = q_{1,3} = q_{2,0} = q_{2,3} = q_{3,0} = q_{3,1} = q_{3,2} = q_{3,3} = 0$.

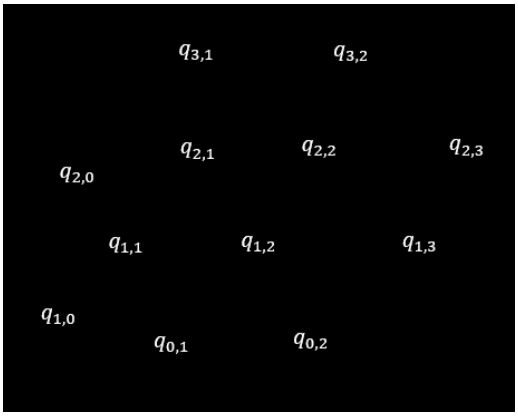

Figure 4. Labelled graph of the simple smart surface structure.

Therefore, the relevant matrixes can be defined as

$$M_2 = \begin{bmatrix} (q_{0,0} - q_{0,0})^2 & \cdots & (q_{0,0} - q_{i,j})^2 & \cdots & (q_{0,0} - q_{3,3})^2 \\ \vdots & \ddots & \vdots & \ddots & \vdots \\ (q_{i,j} - q_{0,0})^2 & \cdots & (q_{i,j} - q_{i,j})^2 & \cdots & (q_{i,j} - q_{3,3})^2 \\ \vdots & \ddots & \vdots & \ddots & \vdots \\ (q_{3,3} - q_{0,0})^2 & \cdots & (q_{3,3} - q_{i,j})^2 & \cdots & (q_{3,3} - q_{3,3})^2 \end{bmatrix}_{16\times16} \tag{23}$$

$$M_4 = \begin{bmatrix} (q_{0,0} - q_{0,0})^4 & \cdots & (q_{0,0} - q_{i,j})^4 & \cdots & (q_{0,0} - q_{3,3})^4 \\ \vdots & \ddots & \vdots & \ddots & \vdots \\ (q_{i,j} - q_{0,0})^4 & \cdots & (q_{i,j} - q_{i,j})^4 & \cdots & (q_{i,j} - q_{3,3})^4 \\ \vdots & \ddots & \vdots & \ddots & \vdots \\ (q_{3,3} - q_{0,0})^4 & \cdots & (q_{3,3} - q_{i,j})^4 & \cdots & (q_{3,3} - q_{3,3})^4 \end{bmatrix}_{16\times16} \tag{24}$$

and so it can be shown that

$$A_1 = \begin{bmatrix} 0&0&0&0&0&0&0&0&0&0&0&0&0&0&0&0 \\ 0&0&0&0&0&1&0&0&0&0&0&0&0&0&0&0 \\ 0&0&0&0&0&0&1&0&0&0&0&0&0&0&0&0 \\ 0&0&0&0&0&0&0&0&0&0&0&0&0&0&0&0 \\ 0&0&0&0&0&1&0&0&0&0&0&0&0&0&0&0 \\ 0&0&0&0&0&0&1&0&0&1&0&0&0&0&0&0 \\ 0&0&0&0&0&0&0&1&0&0&1&0&0&0&0&0 \\ 0&0&0&0&0&0&0&0&0&0&0&0&0&0&0&0 \\ 0&0&0&0&0&0&0&0&0&1&0&0&0&0&0&0 \\ 0&0&0&0&0&0&0&0&0&0&1&0&0&1&0&0 \\ 0&0&0&0&0&0&0&0&0&0&0&1&0&0&1&0 \\ 0&0&0&0&0&0&0&0&0&0&0&0&0&0&0&0 \\ 0&0&0&0&0&0&0&0&0&0&0&0&0&0&0&0 \\ 0&0&0&0&0&0&0&0&0&0&0&0&0&0&0&0 \\ 0&0&0&0&0&0&0&0&0&0&0&0&0&0&0&0 \\ 0&0&0&0&0&0&0&0&0&0&0&0&0&0&0&0 \end{bmatrix}_{16\times16} \tag{25}$$

$$A_\mu = \begin{bmatrix} 0 & \cdots & 0 & \cdots & 0 \\ \vdots & \ddots & \vdots & \ddots & \vdots \\ 0 & \cdots & 0 & \cdots & \mu_{i,j,n,n} \\ \vdots & \ddots & \vdots & \ddots & \vdots \\ 0 & \cdots & 0 & \cdots & 0 \end{bmatrix}_{16\times16} \tag{26}$$

We use two different relationships μ_1 and μ_2 to construct the matrix A_μ, where μ_1 defines the relationship between free nodes and boundary nodes and μ_2 defines the relationship between free nodes each other. Equation (25) can be therefore rewritten as

$$A_1 = \begin{bmatrix}
0&0&0&0&0&0&0&0&0&0&0&0&0&0&0&0\\
0&0&0&0&0&\mu_1&0&0&0&0&0&0&0&0&0&0\\
0&0&0&0&0&0&\mu_1&0&0&0&0&0&0&0&0&0\\
0&0&0&0&0&0&0&0&0&0&0&0&0&0&0&0\\
0&0&0&0&0&\mu_1&0&0&0&0&0&0&0&0&0&0\\
0&0&0&0&0&0&\mu_2&0&0&\mu_2&0&0&0&0&0&0\\
0&0&0&0&0&0&0&\mu_1&0&0&\mu_2&0&0&0&0&0\\
0&0&0&0&0&0&0&0&0&0&0&0&0&0&0&0\\
0&0&0&0&0&0&0&0&0&\mu_1&0&0&0&0&0&0\\
0&0&0&0&0&0&0&0&0&0&\mu_2&0&0&\mu_1&0&0\\
0&0&0&0&0&0&0&0&0&0&0&\mu_1&0&0&\mu_1&0\\
0&0&0&0&0&0&0&0&0&0&0&0&0&0&0&0\\
0&0&0&0&0&0&0&0&0&0&0&0&0&0&0&0\\
0&0&0&0&0&0&0&0&0&0&0&0&0&0&0&0\\
0&0&0&0&0&0&0&0&0&0&0&0&0&0&0&0\\
0&0&0&0&0&0&0&0&0&0&0&0&0&0&0&0
\end{bmatrix}_{16\times16} \tag{27}$$

Through using Eq. (20), the same expression for the potential energy can be found as with Eq. (9). Therefore, the equations of motion can be written as

$$\begin{bmatrix} \ddot{q}_{1,1} \\ \ddot{q}_{1,2} \\ \ddot{q}_{2,1} \\ \ddot{q}_{2,2} \end{bmatrix} = \begin{bmatrix} 2\mu_1 q_{1,1} + \mu_2(2q_{1,1} - q_{2,1} - q_{1,2}) \\ 2\mu_1 q_{1,2} + \mu_2(2q_{1,2} - q_{2,2} - q_{1,1}) \\ 2\mu_1 q_{2,1} + \mu_2(2q_{2,1} - q_{1,1} - q_{2,2}) \\ 2\mu_1 q_{2,2} + \mu_2(2q_{2,2} - q_{1,2} - q_{2,1}) \end{bmatrix} + \begin{bmatrix} -2{q_{1,1}}^3 - (q_{1,1} - q_{2,1})^3 - (q_{1,1} - q_{1,2})^3 \\ -2{q_{1,2}}^3 - (q_{1,2} - q_{2,2})^3 + (q_{1,1} - q_{1,2})^3 \\ -2{q_{2,1}}^3 + (q_{1,1} - q_{2,1})^3 - (q_{2,1} - q_{2,2})^3 \\ -2{q_{2,2}}^3 + (q_{1,2} - q_{2,2})^3 + (q_{2,1} - q_{2,2})^3 \end{bmatrix} \tag{28}$$

Solving $\nabla_q V(\boldsymbol{q}) = 0$ yields a number of equilibria for different values of μ_1 and μ_2, as shown in Fig. 5. Although only $\mu_1 > 0$ is considered in the subsequent analysis, for completeness the number of equilibria is shown for $-2 < \mu_2 < 2$. It can be seen that the total number of equilibria varies with the coupling parameter μ_2. In addition, the maximum number of equilibria occur when $\mu_2 = \mu_1 = 1$, which is found to be 101. It is clear that these equilibria are both stable and unstable and in principle may be connected through paths in the phase of the problem. One type of path is the heteroclinic connection which connects equal-energy unstable equilibria through their stable and unstable manifolds. Therefore, in order to explore all possible equilibrium configurations of the smart surface model the case $\mu_2 = \mu_1 = 1$ for the coupling parameters is used. The case $\mu_2 > \mu_1$ is used later to explore possible reconfigurations between different unstable states of the structure.

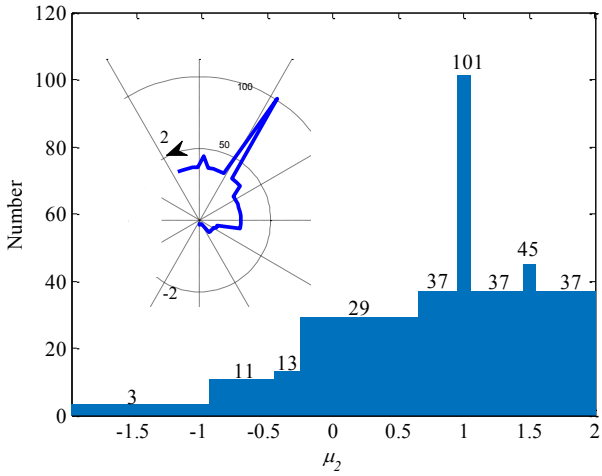

Figure 5. Number of equilibria of the smart surface structure with varying coupling parameter μ_2 with $\mu_1 = 1$.

The equilibrium configurations of the smart surface model are listed in Table 1. The linear stability properties of these equilibria can then be determined through linearisation of Hamilton's equations in the neighbourhood of each equilibrium point by an eigenvalue approach. Through dynamical system theory [34], a set of stable equilibria are then associated with conjugate imaginary eigenvalues and a set of unstable equilibria are associated with real eigenvalues of opposite sign. The linearisation of Hamilton's equations for some general equilibrium point $(\tilde{q}_{1,1}, \tilde{q}_{1,2}, \tilde{q}_{2,1}, \tilde{q}_{2,2})$ of the 4 degree-of-freedom system can be expressed in matrix form as

$$\begin{bmatrix} \ddot{q}_{1,1} \\ \ddot{q}_{1,2} \\ \ddot{q}_{2,1} \\ \ddot{q}_{2,2} \end{bmatrix} = (\mathbf{K} + \mathbf{R}) \begin{bmatrix} q_{1,1} - \tilde{q}_{1,1} \\ q_{1,2} - \tilde{q}_{1,2} \\ q_{2,1} - \tilde{q}_{2,1} \\ q_{2,2} - \tilde{q}_{2,2} \end{bmatrix} \tag{29}$$

$$\mathbf{K} = \begin{bmatrix} \tilde{\gamma}_{1,2}^{1,1} - \tilde{\gamma}_{2,1}^{1,1} - 6\tilde{q}_{1,1}{}^2 & \tilde{\gamma}_{1,2}^{1,1} & \tilde{\gamma}_{2,1}^{1,1} & 0 \\ \tilde{\gamma}_{1,2}^{1,1} & \tilde{\gamma}_{1,2}^{1,1} - \tilde{\gamma}_{2,2}^{1,2} - 6\tilde{q}_{1,2}{}^2 & 0 & \tilde{\gamma}_{2,2}^{1,2} \\ \tilde{\gamma}_{2,1}^{1,1} & 0 & \tilde{\gamma}_{2,1}^{1,1} - \tilde{\gamma}_{2,2}^{2,1} - 6\tilde{q}_{21}{}^2 & \tilde{\gamma}_{2,2}^{2,1} \\ 0 & \tilde{\gamma}_{2,2}^{1,2} & \tilde{\gamma}_{2,2}^{2,1} & \tilde{\gamma}_{2,2}^{1,2} - \tilde{\gamma}_{2,2}^{2,1} - 6\tilde{q}_{2,2}{}^2 \end{bmatrix} \tag{29a}$$

$$\mathbf{R} = \begin{bmatrix} 2\mu_1 + 2\mu_2 & -\mu_2 & -\mu_2 & 0 \\ -\mu_2 & 2\mu_1 + 2\mu_2 & 0 & -\mu_2 \\ -\mu_2 & 0 & 2\mu_1 + 2\mu_2 & -\mu_2 \\ 0 & -\mu_2 & -\mu_2 & 2\mu_1 + 2\mu_2 \end{bmatrix} \tag{29b}$$

where $\tilde{\gamma}_{m,n}^{i,j} = 3(\tilde{q}_{i,j} - \tilde{q}_{m,n})^2$.

The eigenvalues of the linear system can then be found to determine local stability properties. It can be shown that this 4 degree-of-freedom system possesses 29 unstable equilibria and 72 stable equilibria, again noted in Table 1.

Table 1. Stability properties of the equilibria with $\mu_1 = \mu_2 = 1$ and the corresponding surface configuration.

Configuration	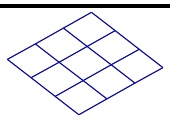	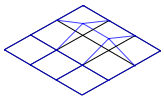	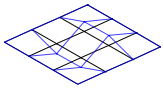	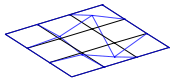	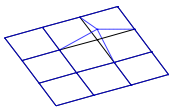
Coordinates	(0 0 0 0)	(0 0 1 1)	(-0.6 0.6 0.6 -0.6)	(-0.1 0.1 -0.6 0.6)	(0 0 0 1)
Potential Energy	0	-1.5	-1.6	-1.1	-1
Type	Maximum	Saddle			
Number	1	28			
Eigenvalues	$\pm 2, \pm 2, \pm\sqrt{2}, \pm\sqrt{6}$	$\pm 1.6, \pm 0.8, \pm 2.1i, \pm 2.6i$	$\pm 1.3, \pm 0.6i, \pm 2.3i, \pm 2.4i$	$\pm 1.4, \pm 1.9, \pm 0.9i, \pm 3.1i$	$\pm 1, \pm 1.1, \pm 2.2, \pm 3.0i$
Configuration	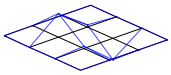	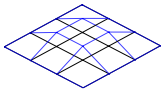	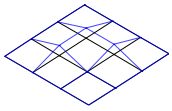	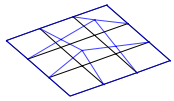	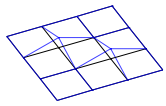
Coordinates	(0.1 1 -1 0.1)	(1 1 1 1)	(0 1 1 1)	(1.2 0.6 0.6 1.2)	(0 1 1 0)
Potential Energy	-2				
Type	Minimum Stable				
Number	72				
Eigenvalues	$\pm 0, \pm 1.2\mathrm{i}, \pm 2.8i, \pm 3.1i$	$\pm 0, \pm\sqrt{2}i, \pm\sqrt{2}i, \pm 2i$	$\pm 0, \pm\sqrt{2}i, \pm 2.2i, \pm 2.6i$	$\pm 0, \pm 0, \pm 2.4i, \pm 2.4i$	$\pm 0, \pm\sqrt{2}i, \pm 2.3i, \pm 3.2i$

4. Heteroclinic connections

In order to explore the possible transition of the model smart surface using heteroclinic connections, several configurations are selected from the set of equilibrium configurations discussed above to act as the initial and final states, respectively. Meanwhile, from Eq. (28) it can be shown that

$$\begin{aligned}\ddot{q}_{1,1} + \ddot{q}_{1,2} + \ddot{q}_{2,1} + \ddot{q}_{2,2} \\ &= 2q_{1,1}\left(\mu_1 - {q_{1,1}}^2\right) + 2q_{1,2}\left(\mu_1 - {q_{1,2}}^2\right) + 2q_{2,1}\left(\mu_1 - {q_{2,1}}^2\right) \\ &+ 2q_{2,2}\left(\mu_1 - {q_{2,2}}^2\right)\end{aligned} \tag{30}$$

so that it can be seen immediately that equilibria can be found at $E_0(0,0,0,0)$, $E_1(\sqrt{\mu_1}, \sqrt{\mu_1}, \sqrt{\mu_1}, \sqrt{\mu_1})$ and $E_2(-\sqrt{\mu_1}, -\sqrt{\mu_1}, -\sqrt{\mu_1}, -\sqrt{\mu_1})$, which shows that these equilibria are independent of μ_2. It can be noted that the stability properties of equilibria E_1 and E_2 are a function of the ratio between μ_2 and μ_1. It can also be shown that the equilibria E_1 and E_2 become unstable for $\mu_2 > \mu_1$. Therefore, E_1 and E_2 will be chosen to be unstable with $\mu_2 > \mu_1$ so that a heteroclinic connection can be found between E_1 and E_2 for illustration. The purpose of finding such a transition is that the unstable equilibria E_1 and E_2 lie on the same potential energy surface and so in principle zero net energy input is needed to reconfigure the structure between them. Then, dynamical system theory can be employed to seek a possible phase space connection between these unstable equilibria. For a conservative system, linearisation of Hamilton's equations in the neighbourhood of each equilibrium point yields pairs of

eigenvalues $\lambda > 0$ and $\lambda < 0$, respectively. These eigenvalues have corresponding eigenvectors associated with the directions $\boldsymbol{u^s}$ and $\boldsymbol{u^u}$. The eigenvectors $\boldsymbol{u^s}$ and $\boldsymbol{u^u}$ are known to be tangent to the stable manifold $\boldsymbol{W}_s$ and the unstable manifold $\boldsymbol{W}_u$ in the neighbourhood of each equilibria [27]. Therefore, the eigenvectors can be mapped to approximate the stable and unstable manifolds by integrating forwards or backwards from an unstable equilibrium point $\boldsymbol{z^e}$, defined by

$$\boldsymbol{z^s} = \boldsymbol{z^e} + \epsilon \boldsymbol{u^s} \tag{31}$$

$$\boldsymbol{z^u} = \boldsymbol{z^e} + \epsilon \boldsymbol{u^u} \tag{32}$$

for $\epsilon \ll 1$. This method can be used find heteroclinic connections between equal-energy unstable equilibria so that the structure can be reconfigured between unstable states. Symmetry is always a basic property for heteroclinic connections in dynamical systems. Therefore, symmetry can be imposed on the problem to search for heteroclinic connections. A two-dimensional space can be obtained by a dimensionality reduction with the following transformation

$$\begin{pmatrix} Q_1 \\ Q_2 \end{pmatrix} = \begin{pmatrix} a_1 & a_2 & a_3 & a_4 \\ b_1 & b_2 & b_3 & b_4 \end{pmatrix} \begin{pmatrix} q_1 \\ q_2 \\ q_3 \\ q_4 \end{pmatrix} \tag{33}$$

where the pre-multiplication matrix is a constant set here to

$$\begin{pmatrix} a_1 & a_2 & a_3 & a_4 \\ b_1 & b_2 & b_3 & b_4 \end{pmatrix} = \begin{pmatrix} 2 & 2 & 2 & 2 \\ 1 & -1 & -1 & 1 \end{pmatrix} \tag{34}$$

thus transforming the four-dimensional space to a two-dimensional space, so that the potential defined in Eq. (9) can be transformed to

$$V(Q,\mu) = (2Q_1 - Q_2)^4 - 2\mu_1(2Q_1 + Q_2)^2 - 2\mu_1(2Q_1 - Q_2)^2 - 8\mu_2 Q_2^2 + 16Q_2^4 + (2Q_1 + Q_2)^4 \tag{35}$$

In this new coordinate system, the equations of motion can be obtained from $\dot{\boldsymbol{P}} = -\nabla_q V(\boldsymbol{Q})$ and so the dynamics of the new system can then be described by

$$\dot{Q}_1 = P_1 \tag{36}$$

$$\dot{P}_1 = 2\mu_1(8Q_1 - 4Q_2) + 2\mu_1(8Q_1 + 4Q_2) - 8(2Q_1 - Q_2)^3 - 8(2Q_1 + Q_2)^3 \tag{37}$$

$$\dot{Q}_2 = P_2 \tag{38}$$

$$\dot{P}_2 = 16\mu_2 Q_2 - 2\mu_1(4Q_1 - 2Q_2) + 2\mu_1(4Q_1 + 2Q_2) - 64Q_2^3 - 4(2Q_1 + Q_2)^3 + 4(2Q_1 - Q_2)^3 \tag{39}$$

In these new coordinates, the system is symmetric about the axis $Q_1 = 0$. The unstable manifold of E_1 is therefore simply the reflection of the stable manifold of E_2, which means that the structure can be reconfigured from state E_1 to state E_2 in principle without energy input. Therefore, a heteroclinic

connection between E_1 and E_2 is symmetric about the axis $Q_1 = 0$, and so must intersect $Q_1 = 0$ perpendicularly, i.e. $\dot{Q}_2 = 0$. The numerical method used to find heteroclinic connection follows McInnes and Waters [27]: for $\mu_2 < 1.2$ and $\mu_1 = 1$, $\dot{Q}_2$ is sufficiently small for an approximate hetercolinic connection to exist. Then when $\mu_2 \approx 1.687$ and $\mu_1 = 1$, an exact hetercolinic connection exists, as is clearly shown in Fig.6. This demonstrates that in principle for an exact value of μ_1 there exist a value of μ_2 not close to μ_1 which admits a heteroclinic path.

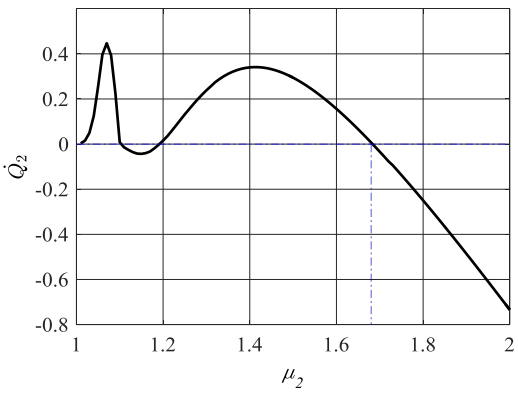

Figure 6. The value of $\dot{Q}_2$ at the first crossing of the unstable manifold with the Q_2 axis, with the increasing parameter μ_2 ($\mu_1 = 1$).

The heteroclinic connection will therefore have a mirror image under $Q_2 \rightarrow -Q_2$, as shown in Fig. 7 and Fig. 8. To initiate the heteroclinic connection, a small disturbance ($\epsilon = 10^{-3}$) is added along the unstable manifold of E_1. For a true heteroclinic connection, motion away from an unstable equilibrium point and towards a connected unstable equilibrium point is asymptotically slow. In practice the actual phase trajectory must shadow the real heteroclinic connection and a controller used to initiate and terminate the heteroclinic connection [29, 30]. The corresponding shape of the surface during the transition from $E_1(1, 1, 1, 1)$ to $E_2(-1, -1, -1, -1)$ is shown in Fig. 9.

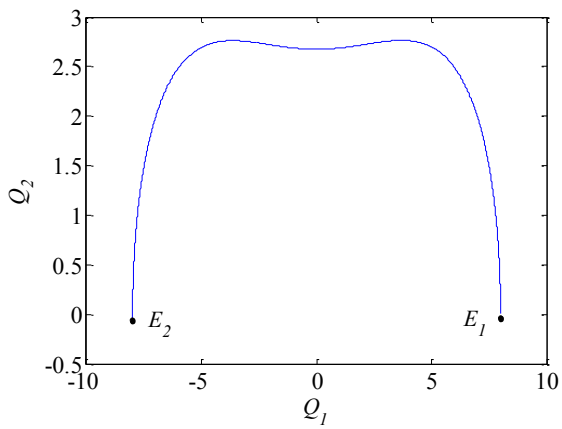

Figure 7. Heteroclinic connection between at E_1 (8, 0) and at E_2 (-8,0) for $\mu_1 = 1$ and $\mu_2 = 1.687\mu_1$. The projection of the phase path in the new coordinate space ($Q_1 - Q_2$).

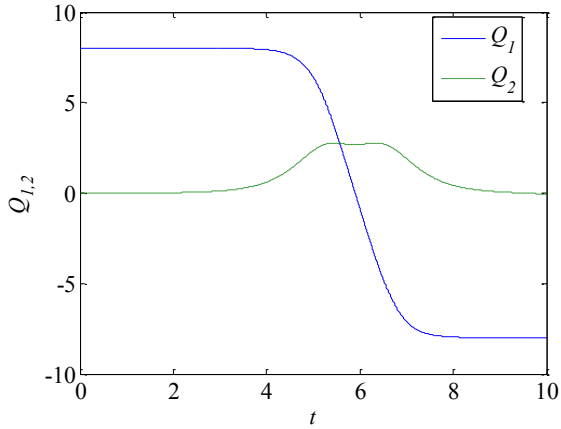

Figure 8. New coordinates $(Q_1 - Q_2)$ for a heteroclinic connection between at E_1 (8, 0) and at E_2 (-8, 0) for $\mu_1 = 1$ and $\mu_2 = 1.687\mu_1$.

Numerical experiments demonstrate that it is in general possible to find a heteroclinic connection for some choice of coupling parameters μ_1 and μ_2, while again a controller [29] can in principle be used to achieve the reconfiguration for a choice of parameters μ_1 and μ_2. Again, in principle for a conservative system without internal dissipation, such reconfigurations do not required the input of energy, which is efficient compared to conventional strategies with transitions between passively stable configurations across a potential barrier.

5. Structure-preserving stabilisation control

This section presents a control method to stabilise the unstable equilibrium configurations of the smart surface structure. For a Hamiltonian system, there exist hyperbolic equilibria that have stable, unstable and center manifolds, with the unstable manifold generating the instability. However, a control law can be applied which will establish Lyapunov stability of the relative motion about the equilibrium point and stabilise an unstable configuration [35,36]. Assuming active control is actuated by the spring coupling parameters (equivalent to modulating their natural length), the dynamics of the controlled system can be written as

$$\begin{bmatrix} \ddot{q}_{1,1} \\ \ddot{q}_{1,2} \\ \ddot{q}_{2,1} \\ \ddot{q}_{2,2} \end{bmatrix} = \boldsymbol{K} \begin{bmatrix} q_{1,1} - \tilde{q}_{1,1} \\ q_{1,2} - \tilde{q}_{1,2} \\ q_{2,1} - \tilde{q}_{2,1} \\ q_{2,2} - \tilde{q}_{2,2} \end{bmatrix} + \boldsymbol{B} \begin{bmatrix} \mu_1 \\ \mu_2 \end{bmatrix} = \boldsymbol{Kq} + \boldsymbol{Bu} \tag{40}$$

$$\mathbf{K} = \begin{bmatrix} \tilde{\gamma}_{1,2}^{1,1} - \tilde{\gamma}_{2,1}^{1,1} - 6\tilde{q}_{1,1}{}^2 & \tilde{\gamma}_{1,2}^{1,1} & \tilde{\gamma}_{2,1}^{1,1} & 0 \\ \tilde{\gamma}_{1,2}^{1,1} & \tilde{\gamma}_{1,2}^{1,1} - \tilde{\gamma}_{2,2}^{1,2} - 6\tilde{q}_{1,2}{}^2 & 0 & \tilde{\gamma}_{2,2}^{1,2} \\ \tilde{\gamma}_{2,1}^{1,1} & 0 & \tilde{\gamma}_{2,1}^{1,1} - \tilde{\gamma}_{2,2}^{2,1} - 6\tilde{q}_{21}{}^2 & \tilde{\gamma}_{2,2}^{2,1} \\ 0 & \tilde{\gamma}_{2,2}^{1,2} & \tilde{\gamma}_{2,2}^{2,1} & \tilde{\gamma}_{2,2}^{1,2} - \tilde{\gamma}_{2,2}^{2,1} - 6\tilde{q}_{2,2}{}^2 \end{bmatrix} \tag{40a}$$

$$\boldsymbol{B} = \begin{bmatrix} 2(q_{1,1} - \tilde{q}_{1,1}) & 2(q_{1,1} - \tilde{q}_{1,1}) - 2(q_{1,2} - \tilde{q}_{1,2}) - 2(q_{2,1} - \tilde{q}_{2,1}) \\ 2(q_{1,2} - \tilde{q}_{1,2}) & 2(q_{1,2} - \tilde{q}_{1,2}) - 2(q_{1,1} - \tilde{q}_{1,1}) - 2(q_{2,2} - \tilde{q}_{2,2}) \\ 2(q_{2,1} - \tilde{q}_{2,1}) & 2(q_{2,1} - \tilde{q}_{2,1}) - 2(q_{1,1} - \tilde{q}_{1,1}) - 2(q_{2,2} - \tilde{q}_{2,2}) \\ 2(q_{2,2} - \tilde{q}_{2,2}) & 2(q_{2,2} - \tilde{q}_{2,2}) - 2(q_{1,2} - \tilde{q}_{1,2}) - 2(q_{2,1} - \tilde{q}_{2,1}) \end{bmatrix} \tag{40b}$$

where $\tilde{\gamma}_{m,n}^{i,j} = 3(\tilde{q}_{i,j} - \tilde{q}_{m,n})^2$.

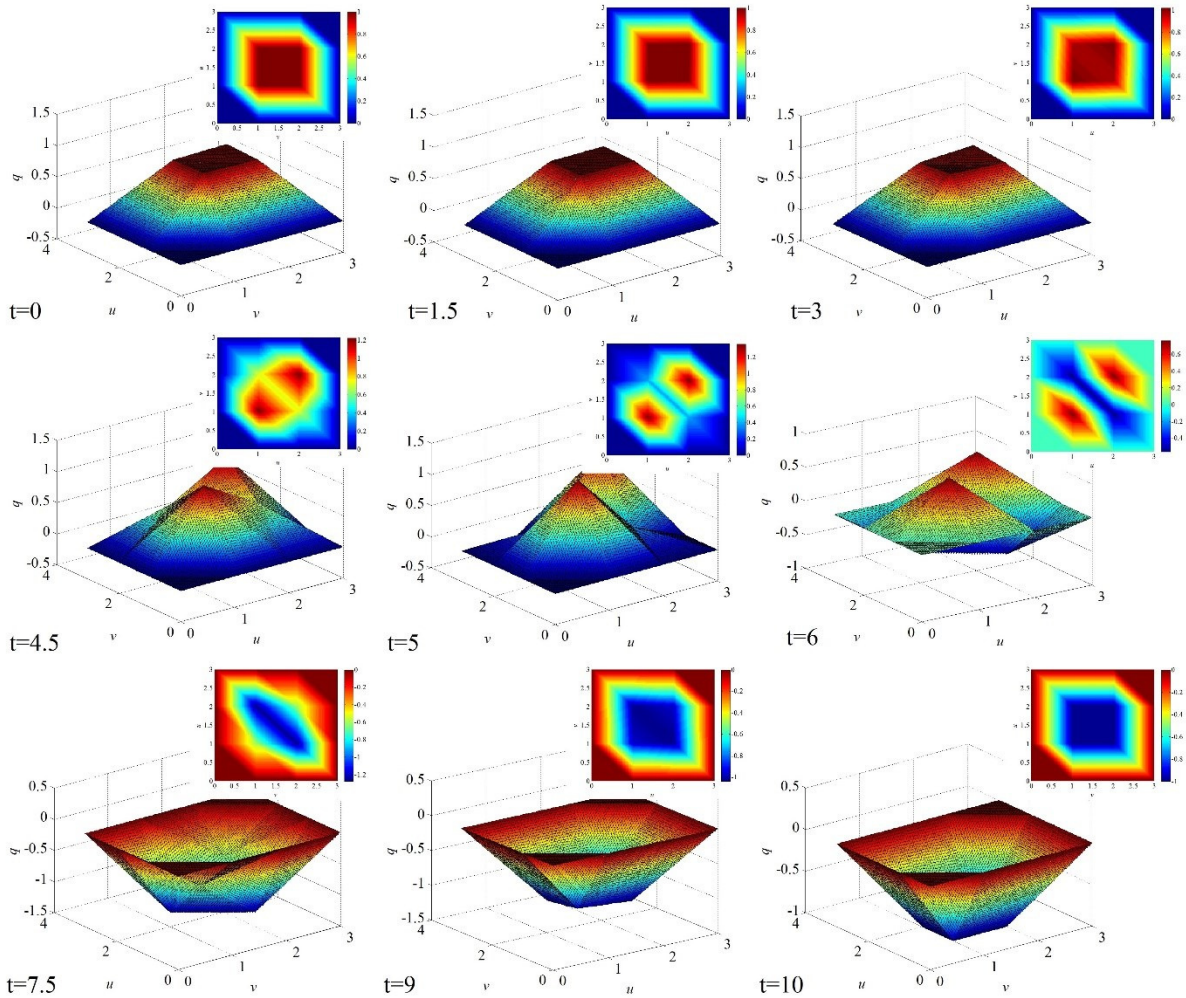

Figure 9. Transition from unstable equilibria E_1 (1, 1, 1, 1) at $t = 0$ to unstable equilibria E_2 (-1, -1, -1, -1,) at $t = 10$ for $\mu_1 = 1$ and $\mu_2 = 1.687\mu_1$.

The controllability matrix [37] for this third-order system is then given by

$$\mathcal{C} = [\boldsymbol{K} \quad \boldsymbol{DK} \quad \boldsymbol{D}^2\boldsymbol{K} \quad \boldsymbol{D}^3\boldsymbol{K}] \tag{41}$$

If the equilibria satisfy the conditions $\tilde{q}_{1,1} \neq \tilde{q}_{1,2} \neq \tilde{q}_{2,1} \neq \tilde{q}_{2,2}$, we can show that $\operatorname{rank} \mathcal{C} = 4$, which implies that the system is fully controllable. However, for the example discussed above in Section 4, it

can be shown that rank $\mathcal{C} = 2$, so that additional actuators are therefore needed to ensure controllability. Therefore, the μ_1 terms (the coupling parameter between each mass and its boundary node) is divided into four parts as μ_{11}, μ_{12}, μ_{13} and μ_{14}, which represent the relationship between corresponding individual masses and their fixed boundaries.

Then the matrix $\boldsymbol{B}$ can then be expressed as

$$\boldsymbol{B} = \begin{bmatrix} \varrho_{1,1} & 0 & 0 & 0 & \varrho_{1,1} - \varrho_{1,2} - \varrho_{2,1} \\ 0 & \varrho_{1,2} & 0 & 0 & \varrho_{1,1} - \varrho_{1,2} - \varrho_{2,1} \\ 0 & 0 & \varrho_{2,1} & 0 & \varrho_{1,1} - \varrho_{1,2} - \varrho_{2,1} \\ 0 & 0 & 0 & \varrho_{2,2} & \varrho_{1,1} - \varrho_{1,2} - \varrho_{2,1} \end{bmatrix} \tag{42}$$

where $\varrho_{i,j} = 2\left(q_{i,j} - \tilde{q}_{i,j}\right)$.

It can then be shown that the controller is constructed as

$$\boldsymbol{T}_c = \{-\sigma^2[G_1\boldsymbol{u}_+\boldsymbol{u}_+^{\boldsymbol{T}} + G_2\boldsymbol{u}_-\boldsymbol{u}_-^{\boldsymbol{T}}] - \varphi^2 G_3[\boldsymbol{u}\boldsymbol{u}^{\boldsymbol{T}} + \overline{\boldsymbol{u}}\overline{\boldsymbol{u}}^{\boldsymbol{T}}]\} \tag{43}$$

where G_1, G_2 and G_3 are the gain parameters, $\boldsymbol{u}_+$ and $\boldsymbol{u}_-$ are the stable and unstable manifolds with corresponding eigenvalues $\pm\sigma$, $\boldsymbol{u}$ and $\overline{\boldsymbol{u}}$ are center manifolds with corresponding eigenvalues are $\pm\varphi i$. A detailed development and proof of the control law can be found elsewhere [35]. This control strategy can work effectively through estimating the relative motion and maintaining the Hamiltonian the structure of the problem. Through Eq. (43) the controller can now stabilise the smart surface to maintain its unstable configuration with the gain parameters $G_1 = 1$, $G_2 = 2$ and $G_3 = 3$, as shown in Fig. 10, with the required controls shown in Fig. 11.

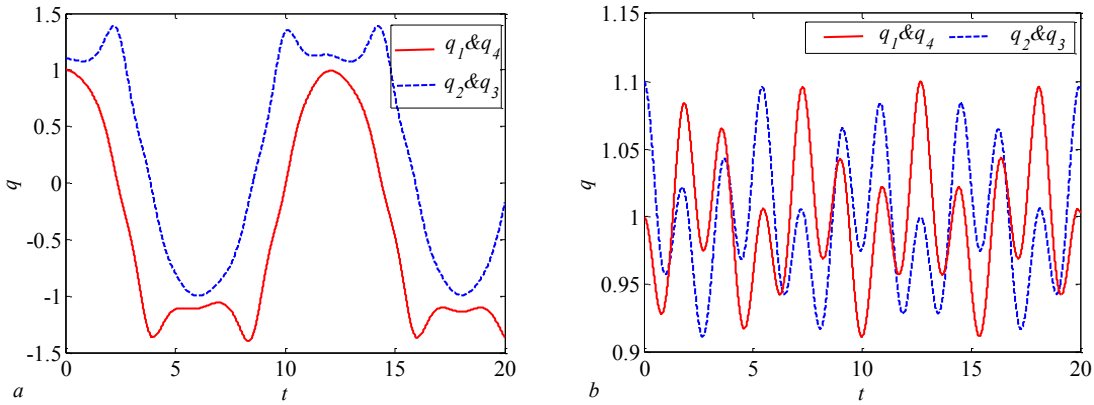

Figure 10. Mass displacements under small disturbance around E_1 (1, 1, 1, 1) (a) without control (b) with control.

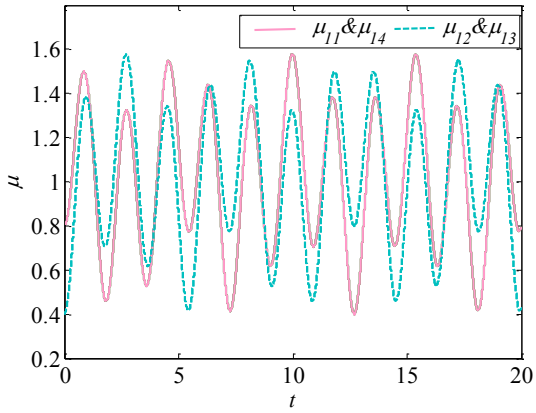

Figure 11. Control actuators generated through the parameters μ_{11}, μ_{12}, $\mu_{13}$and μ_{14}.

A structure preserving controller has therefore been developed to stabilise the smart surface in an unstable configuration, and verified as effective numerically with suitable controls found. The controller is based on computing the local stability characteristics of the motion through the manifolds, which can in principle be realised through modulation of embedded smart materials (e.g. shape memory alloys) to manipulate the spring coupling parameters. Clearly, for a realistic smart surface energy is expended by the controller in maintaining the structure in an unstable equilibrium configuration, between reconfigurations using heteroclinic connections. We therefore envisage the reconfiguration methodology proposed being used for applications where the structure has to frequently reconfigure between different configurations, for example for optical switching. In this way the energy efficiency of the heteroclinic connections for reconfiguration can compensate for the energy expenditure by the controller while temporarily in an actively controlled unstable state.

6. Connected smart surface units

The analysis from the previous section can now be used as the basis for the integration of connected smart surface elements. Such integrated systems can be extended to many potential applications which need frequent state switching to reduce mean power consumption and waste heat dissipation. One important potential application of this integrated smart surface system is that it can be reconfigured between two states to provide motion, for example in a conveyer system, to move an object towards a goal position through arranging sufficient numbers of smart surface units.

It is instructive to consider an analogue model consisting of two smart surfaces to understand the general behaviour of smart surface units connected in series. As shown in Fig. 12, the two adjacent smart surface units are connected by rigid links, which provides a relationship between each mass of every smart surface unit. When a vertical displacement (δ_1, δ_2) is applied in unit 1, unit 2 will move with a corresponding displacement. The motion of the coupled system can then be described by

$$q_{u1,1} = q_{u2,1} = \delta_1 \tag{44}$$

$$q_{u1,2} = q_{u2,2} = \delta_1 \tag{45}$$

$$\ddot{\delta}_1 = \ddot{q}_{u1,1} + \ddot{q}_{u2,1} \tag{46}$$

$$\ddot{\delta}_1 = \ddot{q}_{u1,2} + \ddot{q}_{u2,2} \tag{47}$$

where $q_{u1,1}$ and $q_{u2,1}$ represent two mass displacements of unit 1 and unit 2, respectively; $q_{u1,2}$ and $q_{u2,2}$ represent the other two mass displacements of unit 1 and unit 2, respectively.

Figure 13 shows the mass displacement of the each unit, which can be considered as a heteroclinic connection of the integrated system. It can be seen that the relevant mass displacements between unit 1 and unit 2 have a rigid relationship, which is shown as the dashed line with the double-headed arrow. The parameters of the model used are the same as the model in Section 4. The corresponding shape of the connected smart surfaces associated with initial and final configurations are shown in Fig. 14. It can be seen that unit 1 is in a saddle configuration initially and then changes to a stable configuration, accompanied with unit 2 being reconfigured from a stable equilibrium to a saddle. With this scheme, the heteroclinic connection can be used for reconfiguring an integrated smart surface which is assembled from distributed smart surface units.

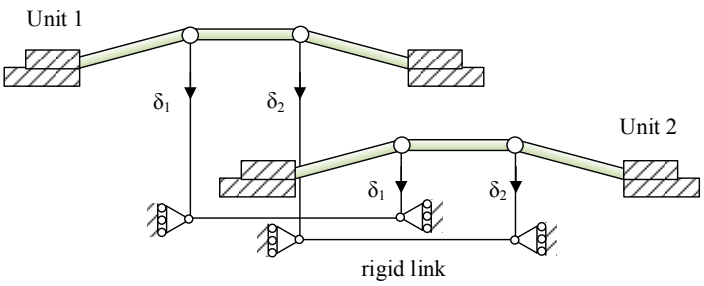

Figure 12. Schematic diagram of two connected smart surface units.

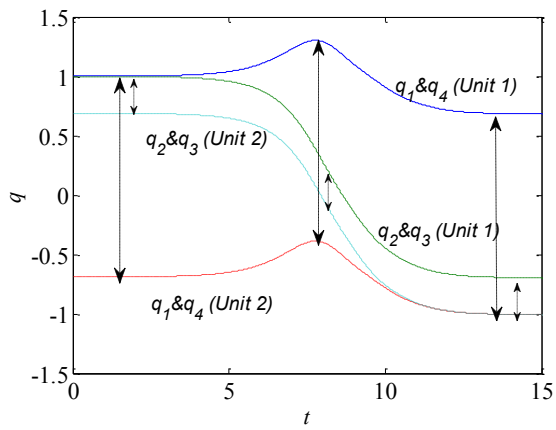

Figure 13. Configuration change during transition from unit 1 to unit 2.

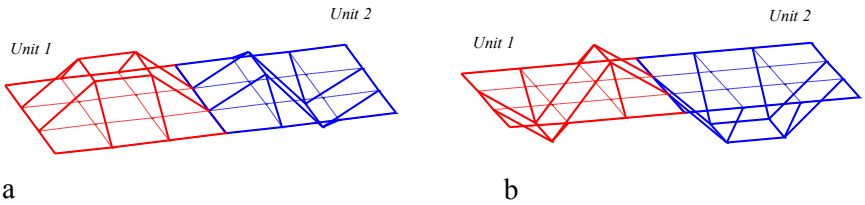

Figure 14. Corresponding shapes of the connected smart surface (a) initial condition (b) final condition.

In the context of our proposed application, the two simply-connected smart surface units can realise reconfigurations as an integrated system. The smart surface unit can transmit motion through connections with neighbouring units. This example is provided to demonstrate how the methodology develop can be used to perform the reconfiguration of a larger smart surface that would be energy efficient compare to traditional approaches with transitions between stable states across a potential barrier.

7. Conclusions

Surface structures possessing multiple equilibria offer interesting dynamical behaviour with a broad range of potential applications. This paper has presented a preliminary study of a simple smart surface model composed of connected masses and linear springs. A general method has been provided to build the equations of motion of such a smart surface system. The theoretical model of the smart surface is nonlinear and complex, but some simple mathematical techniques can be employed to obtain a more compact normalized form. The nonlinear characteristics of the model can therefore be found by using dynamical system theory, which provides a predictive basis for the subsequent analysis of reconfiguring the smart surface and the design of structure-preserving stabilisation control. Then, an active reconfiguration scheme has been investigated to connect equal-energy unstable (but actively controlled) configurations for the purpose of energy-efficient morphing of the smart surface. The reconfiguration of the smart surface between two unstable states does not in principle need additional energy input compared to reconfiguration between two stable configurations. In order to demonstrate that the structure can be actively controlled in an unstable state, a control strategy has been proposed to stabilise the unstable configuration. This control method establishes Lyapunov stability of the relative motion about the equilibrium point and stabilises an unstable configuration. A further development of the smart surface is proposed as an integral system, where the smart surface is extended by forming a series of connected smart surface units. The investigation into the reconfiguration of connected smart surface units can therefore be developed to design larger smart surfaces composed of many more units, which can be used for further applications, such as for conveying, sorting and positioning micro-parts. The purpose of the paper has not been specifically to analyse a high fidelity model of a real smart surface,

but more generally to explore a new concept for reconfiguring smart surfaces using heteroclinic connections between unstable states.

Data accessibility. All data are contained within the published paper.

Authors' contributions. J.Z. carried out the analysis and wrote the manuscript; C.R.M and M.X. provided technical input and gave final approval for publication.

Competing interests. The authors have no competing interests.

Funding. J.Z. is supported by a University of Strathclyde scholarship，C.R.M. is supported by a Royal Society Wolfson Research Merit Award while M.X. is supported by a China Scholarship Council Fellowship.

References

1. Santer, M. & Pellegrino, S. 2008 Compliant multistable structural elements. *Int. J. Solids Struct.* **45**, 6190–6204. (doi:10.1016/j.ijsolstr.2008.07.014)
2. Howell, L. L., Magleby, S. P. & Olsen, B. M. 2013 *Handbook of Compliant Mechanisms*. John Wiley & Sons. (doi:10.1002/9781118516485)
3. Chen, Z., Guo, Q., Majidi, C., Chen, W., Srolovitz, D. J. & Haataja, M. P. 2012 Nonlinear geometric effects in mechanical bistable morphing structures. *Phys. Rev. Lett.* **109**. (doi:10.1103/PhysRevLett.109.114302)
4. Hogg, T. & Huberman, B. A. 1998 Controlling smart matter. *Smart Mater. Struct.* **7**, R1–R14. (doi:10.1088/0964-1726/7/1/001)
5. Guenther, O., Hogg, T. & Huberman, B. A. 1997 Controls for unstable structures. In *Smart Structures and Materials 1997: Mathematics and Control in Smart Structures, The Society of Photo-Optical Instrumentation Engineers (SPIE) conf. (June); Proc.SPIE*, pp. 754–763.(doi:10.1117/12.276594)
6. Lagoudas, D. C. 2008 *Shape Memory Alloys: Modeling and Engineering Applications*. New York: Springer.
7. Flatau, A. B. & Chong, K. P. 2002 Dynamic smart material and structural systems. *Eng. Struct.* **24**, 261–270. (doi:10.1016/S0141-0296(01)00093-1)
8. Mohd Jani, J., Leary, M., Subic, A. & Gibson, M. a. 2014 A review of shape memory alloy research, applications and opportunities. *Mater. Des.* **56**, 1078–1113. (doi:10.1016/j.matdes.2013.11.084)
9. Behl, M., Kratz, K., Zotzmann, J., Nöchel, U. & Lendlein, A. 2013 Reversible bidirectional shape-memory polymers. *Adv. Mater.* **25**, 4466–4469. (doi:10.1002/adma.201300880)
10. Behl, M., Kratz, K., Noechel, U., Sauter, T. & Lendlein, A. 2013 Temperature-memory polymer actuators. *Proc. Natl. Acad. Sci. U. S. A.* **110**, 12555–9. (doi:10.1073/pnas.1301895110)
11. Hurlebaus, S. & Gaul, L. 2006 Smart structure dynamics. *Mech. Syst. Signal Process.* **20**, 255–281. (doi:10.1016/j.ymssp.2005.08.025)
12. Datashvili, L., Baier, H., Wei, B., Endler, S. & Schreider, L. 2013 Design of a Morphing Skin Using Flexible Fiber Composites for Space-Reconfigurable Reflectors. *54th AIAA/ASME/ASCE/AHS/ASC Struct. Struct. Dyn. Mater. Conf.* , 1–11. (doi:10.2514/6.2013-1522)
13. Mazzone, A., Spagno, C. & Kunz, A. 2004 The HoverMesh: A deformable structure based on vacuum cells. *Proc. ACM SIGCHI Int. Conf. Adv. Comput. Entertain. Technol.* , 187–193. (doi:10.1145/1067343.1067366)
14. Shi, M., Zhang, J., Chen, H., Han, M., Shankaregowda, S. A., Su, Z., Meng, B., Cheng, X. & Zhang, H. 2016 Self-Powered Analogue Smart Skin. *ACS Nano* **10**, 4083–91. (doi:10.1021/acsnano.5b07074)

15. De Focatiis, D. S. a & Guest, S. D. 2002 Deployable membranes designed from folding tree leaves. *Philos. Trans. A. Math. Phys. Eng. Sci.* **360**, 227–238. (doi:10.1098/rsta.2001.0928)

16. Yoo, E.-J., Roh, J.-H. & Han, J.-H. 2007 Wrinkling control of inflatable booms using shape memory alloy wires. *Smart Mater. Struct.* **16**, 340–348. (doi:10.1088/0964-1726/16/2/012)

17. Hawkes, E., An, B., Benbernou, N. M., Tanaka, H., Kim, S., Demaine, E. D., Rus, D. & Wood, R. J. 2010 Programmable matter by folding. *Proc. Natl. Acad. Sci. U. S. A.* **107**, 12441–12445. (doi:10.1073/pnas.0914069107)

18. Cui, Y. & Santer, M. 2015 Highly multistable composite surfaces. *Compos. Struct.* **124**, 44–45. (doi:10.1016/j.compstruct.2014.12.052)

19. Shaw, L. A. & Hopkins, J. B. 2015 An actively controlled shape-morphing compliant microarchitectured material. *J. Mech. Robot.* **8**, 21019. (doi:10.1115/1.4031168)

20. Wu, J. & Burgueño, R. 2006 An integrated approach to shape and laminate stacking sequence optimization of free-form FRP shells. *Comput. Methods Appl. Mech. Eng.* **195**, 4106–4123. (doi:10.1016/j.cma.2005.07.015)

21. Hu, N. & Burgueño, R. 2015 Elastic postbuckling response of axially-loaded cylindrical shells with seeded geometric imperfection design. *Thin-Walled Struct.* **96**, 256–268. (doi:10.1016/j.tws.2015.08.014)

22. Bornengo, D., Scarpa, F. & Remillat, C. 2005 Evaluation of hexagonal chiral structure for morphing airfoil concept. *Proc. Inst. Mech. Eng. Part G J. Aerosp. Eng.* **219**, 185–192. (doi:10.1243/095441005X30216)

23. Neville, R. M., Scarpa, F. & Pirrera, A. 2016 Shape morphing Kirigami mechanical metamaterials. *Sci. Rep.* **6**, 31067. (doi:10.1038/srep31067)

24. Schenk, M. & Guest, S. D. 2013 Geometry of Miura-folded metamaterials. *Proc. Natl. Acad. Sci. U. S. A.* **110**, 3276–81. (doi:10.1073/pnas.1217998110)

25. Previtali, F., Arrieta, A. F. & Ermanni, P. 2015 Double-walled corrugated structure for bending-stiff anisotropic morphing skins. *J. Intell. Mater. Syst. Struct.* **26**, 599–613. (doi:10.1177/1045389X14554132)

26. El Baz, D., Boyer, V., Bourgeois, J., Dedu, E. & Boutoustous, K. 2012 Distributed part differentiation in a smart surface. *Mechatronics* **22**, 522–530. (doi:10.1016/j.mechatronics.2011.05.005)

27. McInnes, C. R. & Waters, T. J. 2008 Reconfiguring smart structures using phase space connections. *Smart Mater. Struct.* **17**, 25030. (doi:10.1088/0964-1726/17/2/025030)

28. McInnes, C. R., Gorman, D. G. & Cartmell, M. P. 2008 Enhanced vibrational energy harvesting using nonlinear stochastic resonance. *J. Sound Vib.* **318**, 655–662. (doi:10.1016/j.jsv.2008.07.017)

29. Zhang, J. & McInnes, C. R. 2015 Reconfiguring smart structures using approximate heteroclinic connections. *Smart Mater. Struct.* **24**, 105034. (doi:10.1088/0964-1726/24/10/105034)

30. Zhang, J. & McInnes, C. R. 2015 Reconfiguring Smart Structures using Approximate Heteroclinic Connections in A Spring-Mass Model. In *Proceedings of the ASME Conference on Smart Materials, Adaptive Structures and Intelligent Systems (SMASIS 2015)*, Colorado Springs.

31. Zhang, J. & McInnes, C. R. 2016 Using Instability to Reconfigure Smart Structures in a Spring-Mass Model. *Mech. Syst. Signal Process.* (*Accepted)* . (doi: 10.1016/j.ymssp.2016.11.029)

32. Zhang, J. & McInnes, C. R. 2016 Reconfiguration of a four-bar mechanism using phase space connections. *Mech. Syst. Signal Process.* (doi:10.1016/j.ymssp.2016.03.024)

33. Turco, E., Dell'Isola, F., Cazzani, A. & Rizzi, N. L. 2016 Hencky-type discrete model for pantographic structures: numerical comparison with second gradient continuum models. *Zeitschrift für Angew. Math. und Phys.* **67**, 85. (doi:10.1007/s00033-016-0681-8)

34. Wiggins, S. 1990 *Introduction to applied nonlinear dynamical systems and chaos*. New York: Springer.

35. Xu, M. & Xu, S. 2009 Structure-Preserving Stabilization for Hamiltonian System and its Applications in Solar Sail. *J. Guid. Control. Dyn.* **32**, 997–1004. (doi:10.2514/1.34757)

36. Xu, M., Zhu, J., Tan, T. & Xu, S. 2012 Application of Hamiltonian structure-preserving control to formation flying on a J 2-perturbed mean circular orbit. *Celest. Mech. Dyn. Astron.* **113**, 403–433. (doi:10.1007/s10569-012-9430-2)

37. Henk., N. & Schaft, A. V. der. 2013 *Nonlinear Dynamical Control Systems*. Springer Science & Business Media. (doi:10.1137/1033066)